NUCLEAR DATA AND MEASUREMENTS SERIES

ANL/NDM-91

On the Energy Dependence of the Optical Model of Neutron Scattering from Niobium

by

A.B. Smith, P.T. Guenther, and R.D. Lawson

May 1985

ARGONNE NATIONAL LABORATORY,
ARGONNE, ILLINOIS 60439, U.S.A.

NUCLEAR DATA AND MEASUREMENTS SERIES

ANL/NDM-91

ON THE ENERGY DEPENDENCE OF THE OPTICAL MODEL OF NEUTRON SCATTERING FROM NIOBIUM*

by

A. B. Smith, P. T. Guenther and R. D. Lawson

May 1985

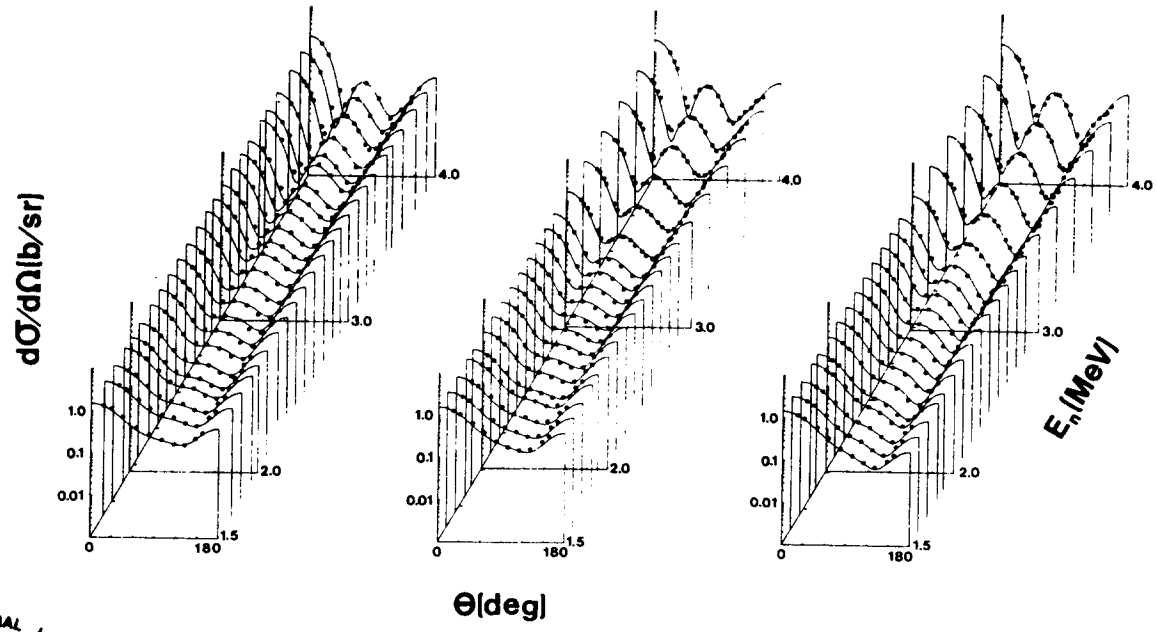

ARGONNE NATIONAL LABORATORY, ARGONNE, ILLINOIS

Operated by THE UNIVERSITY OF CHICAGO

for the U. S. DEPARTMENT OF ENERGY

under Contract W-31-109-Eng-38

ANL/NDM-91

ON THE ENERGY DEPENDENCE OF THE OPTICAL MODEL OF NEUTRON SCATTERING FROM NIOBIUM*

by

A. B. Smith, P. T. Guenther and R. D. Lawson
May 1985

NEUTRON SCATTERING. Measured $d\sigma/d\Omega(n)$, 1.5-10.0 MeV, 20-160 deg., Optical-model interpretation. Determined energy dependencies of volume integrals of real and imaginary potentials.

*This work supported by the U. S. Department of Energy

Applied Physics Division
Argonne National Laboratory
9700 S. Cass Avenue
Argonne, Illinois 60439
USA

NUCLEAR DATA AND MEASUREMENTS SERIES

The Nuclear Data and Measurements Series presents results of studies in the field of microscopic nuclear data. The primary objective is the dissemination of information in the comprehensive form required for nuclear technology applications. This Series is devoted to: a) measured microscopic nuclear parameters, b) experimental techniques and facilities employed in measurements, c) the analysis, correlation and interpretation of nuclear data, and d) the evaluation of nuclear data. Contributions to this Series are reviewed to assure technical competence and, unless otherwise stated, the contents can be formally referenced. This Series does not supplant formal journal publication but it does provide the more extensive information required for technological applications (e.g., tabulated numerical data) in a timely manner.

INFORMATION ABOUT OTHER ISSUES IN THE ANL/NDM SERIES:

A list of titles and authors for reports ANL/NDM-1 through ANL/NDM-50 can be obtained by referring to any report of this series numbered ANL/NDM-51 through ANL/NDM-76. Requests for a complete list of titles or for copies of previous reports should be directed to:

Section Secretary
Applied Nuclear Physics Section
Applied Physics Division
Building 316
Argonne National Laboratory
9700 South Cass Avenue
Argonne, Illinois 60439
USA

ANL/NDM-51 Measured and Evaluated Neutron Cross Sections of Elemental Bismuth by A. Smith, P. Guenther, D. Smith and J. Whalen, April 1980.

ANL/NDM-52 Neutron Total and Scattering Cross Sections of ^{6}Li in the Few MeV Region by P. Guenther, A. Smith and J. Whalen, February 1980.

ANL/NDM-53 Neutron Source Investigations in Support of the Cross Section Program at the Argonne Fast-Neutron Generator by James W. Meadows and Donald L. Smith, May 1980.

ANL/NDM-54 The Nonelastic-Scattering Cross Sections of Elemental Nickel by A. B. Smith, P. T. Guenther and J. F. Whalen, June 1980.

ANL/NDM-55 Thermal Neutron Calibration of a Tritium Extraction Facility using the $^{6}Li(n,t)^{4}He/^{197}Au(n,\gamma)^{198}Au$ Cross Section Ratio for Standardization by M. M. Bretscher and D. L. Smith, August 1980.

ANL/NDM-56 Fast-Neutron Interactions with ^{182}W, ^{184}W and ^{186}W by P. T. Guenther, A. B. Smith and J. F. Whalen, December 1980.

ANL/NDM-57 The Total, Elastic- and Inelastic-Scattering Fast-Neutron Cross Sections of Natural Chromium by Peter T. Guenther, Alan B. Smith and James F. Whalen, January 1981.

ANL/NDM-58 Review of Measurement Techniques for the Neutron Capture Process by W. P. Poenitz, August 1981.

ANL/NDM-59 Review of the Importance of the Neutron Capture Process in Fission Reactors by Wolfgang P. Poenitz, July 1981.

ANL/NDM-60 Gamma-Ray Detector Calibration Methods Utilized in the Argonne FNG Group Activation Cross Section Measurement Program by James W. Meadows and Donald L. Smith, April 1984

ANL/NDM-61 Fast-neutron Total and Scattering Cross Sections of ^{58}Ni by Carl Budtz-Jørgensen, Peter T. Guenther, Alan B. Smith and James F. Whalen, September 1981.

ANL/NDM-62 Covariance Matrices and Applications to the Field of Nuclear Data by Donald L. Smith, November 1981.

ANL/NDM-63 On Neutron Inelastic-Scattering Cross Sections of ^{232}Th, ^{233}U, ^{235}U, ^{238}U, ^{239}U, and ^{239}Pu and ^{240}Pu by Alan B. Smith and Peter T. Guenther, January 1982.

ANL/NDM-64 The Fission-Fragment Angular Distributions and Total Kinetic Energies for $^{235}U(n,f)$ from 0.18 to 8.83 MeV by James W. Meadows and Carl Budtz-Jørgensen, January 1982.

ANL/NDM-65 Note on the Elastic Scattering of Several-MeV Neutrons from Elemental Calcium by Alan B. Smith and Peter T. Guenther, March 1982.

ANL/NDM-66 Fast-neutron Scattering Cross Sections of Elemental Silver by Alan B. Smith and Peter T. Guenther, May 1982.

ANL/NDM-67 Non-evaluation Applications for Covariance Matrices by Donald L. Smith, July 1982.

ANL/NDM-68 Fast-neutron Total and Scattering Cross Sections of ^{103}Rh by Alan B. Smith, Peter T. Guenther and James F. Whalen, July 1982.

ANL/NDM-69 Fast-neutron Scattering Cross Sections of Elemental Zirconium by Alan B. Smith and Peter T. Guenther, December 1982.

ANL/NDM-70 Fast-neutron Total and Scattering Cross Sections of Niobium by Alan B. Smith, Peter T. Guenther and James F. Whalen, July 1982.

ANL/NDM-71 Fast-neutron Total and Scattering Cross Sections of Elemental Palladium by Alan B. Smith, Peter T. Guenther and James F. Whalen, June 1982.

ANL/NDM-72 Fast-neutron Scattering from Elemental Cadmium by Alan B. Smith and Peter T. Guenther, July 1982.

ANL/NDM-73 Fast-neutron Elastic-Scattering Cross Sections of Elemental Tin by C. Budtz-Jørgensen, Peter T. Guenther and Alan B. Smith, July 1982.

ANL/NDM-74 Evaluation of the ^{238}U Neutron Total Cross Section by Wolfgang Poenitz, Alan B. Smith and Robert Howerton, December 1982.

ANL/NDM-75 Neutron Total and Scattering Cross Sections of Elemental Antimony by A. B. Smith, P. T. Guenther and J. F. Whalen, September 1982.

ANL/NDM-76 Scattering of Fast-Neutrons from Elemental Molybdenum by Alan B. Smith and Peter T. Guenther, November 1982.

ANL/NDM-77 A Least-Squares Method for Deriving Reaction Differential Cross Section Information from Measurements Performed in Diverse Neutron Fields by Donald L. Smith, November 1982.

ANL/NDM-78 Fast-Neutron Total and Elastic-Scattering Cross Sections of Elemental Indium by A. B. Smith, P. T. Guenther, and J. F. Whalen, November 1982.

ANL/NDM-79 Few-MeV Neutrons Incident on Yttrium by C. Budtz-Jørgensen, P. Guenther, A. Smith and J. Whalen, June 1983.

ANL/NDM-80 Neutron Total Cross Section Measurements in the Energy Region from 47 keV to 20 MeV by W. P. Poenitz and J. F. Whalen, July 1983.

ANL/NDM-81 Covariances for Neutron Cross Sections Calculated Using a Regional Model Based on Elemental-Model Fits to Experimental Data by D. L. Smith and P. T. Guenther, November 1983.

ANL/NDM-82 Reaction Differential Cross Sections from the Least-Squares Unfolding of Ratio Data Measured in Diverse Neutron Fields by D. L. Smith, January 1984.

ANL/NDM-83 The Fission Cross Sections of Some Thorium, Uranium, Neptunium and Plutonium Isotopes Relative to ^{235}U by J. W. Meadows, October 1983.

ANL/NDM-84 ^{235}U and ^{239}Pu Sample-Mass Determinations and Intercomparisons by W. P. Poenitz and J. W. Meadows, November 1983.

ANL/NDM-85 Measurement of the $^{51}V(n,p)^{51}Ti$ Reaction Cross Section from Threshold to 9.3 MeV by the Activation Method by D. L. Smith, J. W. Meadows and I. Kanno, June 1984.

ANL/NDM-86 Energy-Differential Cross Section Measurement for the $^{51}V(n,\alpha)^{48}Sc$ Reaction by I. Kanno, J. W. Meadows, and D. L. Smith, July 1984.

ANL/NDM-87 Cross-Section Measurement for the $^{7}Li(n,n't)^{4}He$ Reaction at 14.74 MeV by D. L. Smith, J. W. Meadows, M. M. Bretscher and S. A. Cox, September 1984.

ANL/NDM-88 An Evaluated Nuclear Data File for Niobium by A. B. Smith, D. L. Smith and R. J. Howerton, March 1985.

ANL/NDM-89 Compilation and Evaluation of 14-MeV Neutron Activation Cross Sections for Nuclear Technology Applications: Set I by Bernard P. Evain, Donald L. Smith and Paul Lucchese, April 1985.

ANL/NDM-90 Fast-Neutron-Spectrum Measurements for the Thick-Target $^{9}Be(d,n)^{10}B$ Reaction at E_d = 7 MeV by D. L. Smith, J. W. Meadows and P. T. Guenther, April 1985

TABLE OF CONTENTS

ON THE ENERGY DEPENDENCE OF THE OPTICAL MODEL OF NEUTRON SCATTERING FROM NIOBIUM*

by

A. B. Smith, P. T. Guenther and R. D. Lawson
Applied Physics Division
Argonne National Laboratory

ABSTRACT

Neutron differential-elastic-scattering cross sections of niobium were measured from 1.5 to 10.0 MeV at intervals of $\leq$ 200 keV below 4.0 MeV, and of $\approx$ 500 keV from 4.0 to 10.0 MeV. Ten to more than fifty differential-cross-section values were determined at each incident energy, distributed over the angular range $\approx$ 20 to 160 degrees. The observed values were interpreted in the context of the spherical optical-statistical model. It was found that the volume integral of the real potential decreased with energy whereas the integral of the imaginary part increased. The energy dependence in both cases was consistent with a linear variation. There is a dispersion relationship between the real and imaginary potentials, and when this was used, in conjunction with the experimental imaginary potential, it was possible to predict the observed energy dependence of the real potential to a good degree of accuracy, thus supporting the consistency of the data and its analysis. The real-potential well depths needed to give the correct binding energies of the $2d_{5/2}$, $3s_{1/2}$, $2d_{3/2}$ and $1g_{7/2}$ particle states and of the $1g_{9/2}$ hole state are in reasonable agreement with those given by a linear extrapolation of the scattering potential. However, the well depths needed to give the observed binding of the $2p_{3/2}$, $1f_{5/2}$ and $2p_{1/2}$ hole states are about 10% less than the extrapolated values.

*This work supported by the U. S. Department of Energy.

I. INTRODUCTION

There has been recent interest in the energy dependence of the optical model (OM) potential near the Fermi surface. It has been theoretically suggested that the energy dependence of the real OM potential deviates from the essentially linear behavior common to most global phenomenological models based upon higher-energy neutron and charged-particle data (1). This deviation is attributed to coupling to low-lying collective states resulting in an effective mass, m*, which is sharply enhanced near the Fermi surface. This leads to a large reduction, or even inversion, of the energy dependence of the real OM potential. From studies of the giant-dipole resonance (particularly in ^{208}Pb), Brown et al. (2) suggest an approximate expression for the energy dependence of the ratio m*/m. This formula is consistent with the higher-energy behavior of the phenomenological global OMs but gives an energy independent real potential near the Fermi surface. Bauer et al. (3) and Hodgson (4) reached similar conclusions from considerations of OMs based upon higher-energy neutron and charged-particle observations and, particularly, the energies of bound single-particle states. Mahaux and Ngô (5) have extensively studied the polarization and correlation contributions to the shell model near the Fermi surface and suggest a highly non-linear energy dependence of the real OM potential near the Fermi surface. These authors illustrate these effects for the closed-shell nuclei ^{40}Ca and ^{208}Pb. They conclude that the imaginary potential is at a minimum at the Fermi surface and rapidly increases as the energy goes either positive or negative with respect to the Fermi energy. They also suggest a real potential consisting of a Hartree-Fock component, upon which are superimposed relatively small polarization and correlation contributions. The net effect is a real potential with an approximately linear energy dependence well away from the Fermi surface (as conventionally found in global phenomenological models), but with a sharp decrease, or even inversion, of the energy dependence as the Fermi surface is approached. The region of most interest is near or below the coulomb barrier and thus largely forbidden to charged-particle studies. It is amenable to fast-neutron investigation, but the available neutron data generally do not have the scope, detail, consistency and/or accuracy necessary for a quantitative test of the above concepts. The above hypotheses have been experimentally examined using neutron data near the doubly closed shell at A=208 by Finlay et al. (6).

A number of the above theoretical concepts are illustrated in the context of the doubly-magic nuclei ^{40}Ca and ^{208}Pb. Neither of these nuclei are experimentally attractive targets for the present purposes as their neutron cross sections in the most interesting few-MeV region fluctuate to such an extent that the derivation of a reliable OM from the observations is speculative (7,8). A far more attractive experimental target is a spherical, medium-weight nucleus (preferably near a closed shell), having a high

level density that will make possible the determination of energy-averaged cross sections, consistent with the concept of the OM, at relatively low energies. One of the very few elemental targets that meet such criteria is niobium. It is readily available, monoisotopic, essentially spherical, has a high level density, and is only two neutrons beyond the N=50 shell. In addition, there is available a body of accurate supporting neutron-total-cross-section information (9). For these reasons, niobium was chosen for the present study. The objectives were the acquisition of detailed elastic-scattering data and, the deduction of an OM potential suitable for testing the above theoretical concepts over an energy region extending from as close to the Fermi surface as possible to the charged-particle region at 10 MeV and above. The data base primarily consists of differential-elastic-scattering cross sections for neutron energies of 1.5 to 10.0 MeV, obtained with good accuracy and considerable detail. The parameters of the OM were derived from these observables.

The experimental methods are briefly outlined in Section II. The experimental results are presented in Section III, and their interpretation given in Section IV. The results are discussed in the context of the above theoretical suggestions in Section V.

II. OUTLINE OF EXPERIMENTAL METHOD

The measurement sample was a 2 cm diameter and 2 cm long cylinder of chemically pure (99+%) metallic niobium (100% ^{93}Nb). Its density was determined using conventional weighing- and dimensional-measurement techniques. Below 4.0 MeV, the measurements were made using the ^{7}Li(p,n)^{7}Be neutron-source reaction (10). Above 4.0 MeV, the D(d,n)^{3}He source reaction was used with a gas cell 3 cm long having a nickel window approximately 3 micro-m thick. The thickness of the lithium-metal target film, or the deuterium pressure of the gas cell, was adjusted to obtain the desired incident-neutron energy spreads. The latter were 50-75 keV below 4.0 MeV (11) and, above 4.0 MeV, decreased from approximately 300 keV at 4.5 MeV to 100 keV at 10.0 MeV. Particularly at the lower energies, these incident-neutron energy spreads were chosen to be rather wide so as to assure that any possible fluctuations in the cross sections were averaged. The energy scale was determined, by control of the incident reaction particle, to accuracies of 10 keV or better. The sources were pulsed at a repetition rate of 2 MHz, with burst durations of approximately 1 nsec.

The neutron differential-elastic-scattering cross sections were measured using the Argonne National Laboratory 10-angle time-of-flight system at the 8 MeV Argonne Tandem Dynamitron Accelerator (12). The scattering sample was placed approximately 13 cm from the source at a zero-degree reaction angle. Ten flight paths, defined by massive collimators, were

distributed between scattering angles of 20 and 160 degrees. The collimator system was rotated so that at least twenty angular settings were used at each energy above 3.0 MeV. Relative scattering angles were known to ± 0.1 degrees, and the absolute scale was determined to approximately ± 0.5 degrees by observation of neutrons scattered from hydrogen both left and right of the center line. The absolute-scale uncertainty implies a geometeric stability of the effective neutron source and the scattering sample of 1 mm. The neutron detectors were proton-recoil scintillators placed approximately 5.1 m from the scattering sample. The relative responses of the detectors were determined by the observation of neutrons emitted in the spontaneous fission of ^{252}Cf (13). Below 4.0 MeV, these relative responses were normalized to the independently-measured neutron total cross sections of carbon, as outlined in ref. 14. This method of normalization implies that the scattering cross sections are essentially independent of any reference standard. Above approximately 4.8 MeV, this method of normalization is not reliable due to a large carbon inelastically-scattered component. Therefore, above 4.0 MeV the relative detector sensitivities were normalized to the concurrently observed H(n,n) scattering, using the well known H(n,n) cross sections (15). It should be noted that the ten detector responses were independently normalized. Thus there is a ten-fold redundancy in the cross section normalization. This, and the speed of the data acquisition, are the power of the system, though the systematic-normalization and statistical uncertainties as a function of angle are not separable and must be properly treated in the interpretation. The elastic-scattering cross sections were deduced from the observed velocity spectra using the data reduction techniques described in ref. 16. These included corrections for multiple-event, beam-attenuation, and angular-resolution effects, using a combination of analytical and Monte-Carlo procedures applied to both the niobium sample and the H(n,n) (polyethylene) and carbon reference samples.

III. EXPERIMENTAL RESULTS

The lower-energy measurements (1.5-4.0 MeV) were made in considerable detail in order to assure that an energy-averaged behavior, consistent with the concept of the OM, was achieved. Toward this end, the above cited 50-75 keV incident-neutron energy resolutions were used. In addition, the results at adjacent energies were averaged in order to further smooth any possible fluctuations. Measurements were made at ten angular increments below 3.0 MeV, and at energy intervals of approximately 50 keV. From 3.0-4.0 MeV, the measurements were made at 20 or more scattering angles and at energy intervals of 200 keV. The statistical uncertainties of the differential cross sections were generally less than 2%. Systematic uncertainties were less than 3%, and those associated with correction procedures generally 1% or less.

Thus the overall uncertainties below 4.0 MeV were generally 5% or less. The details of the measurements below 4.0 MeV have been previously reported (11).

Above 4.0 MeV the measurements were made at incident-neutron energy intervals of approximately 500 keV to 10.0 MeV, and at a minimum of 20 scattering angles. All the distributions were measured at least twice at widely separated measurement periods, and some four times, with good reproducibility. This reproducibility is illustrated in Fig. 1 where four sets of data are superimposed. The statistical accuracies of the measured cross sections varied from a fraction of a percent at small scattering angles, to ten percent or more at the extreme minima of the distributions. Systematic normalization uncertainties were generally estimated to be approximately 3%, and correction procedures introduced a further uncertainty of approximately 1%, except at the minima of the distributions where the corrections were less reliable. Throughout the higher-energy measurements, it was assumed that the minimum experimental uncertainty was 1.5 mb and that was often the dominant uncertainty at the minima of the distributions.

All the uncertainty estimates do not include contributions from the angular uncertainty cited above. In most cases, those contributions are relatively small, but they can be very significant at the forward scattering angles and the higher energies, as discussed in Section IV.

All of the measured differential-"elastic-scattering" cross sections included an inelastically-scattered contribution is due to the excitation of the 30-keV metastable state (17). This contribution was very small as the spin change involved is large and there are a number of channels open to the decay of the compound nucleus throughout the energy range of the present experiments. The requisite small correc tions to the measured elastic-scattering distributions due to the inelastic contribution were made in the interpretation described below. In addition to the elastic-scattering results, broad-resolution inelastic-scattering cross sections were determined at incident neutron energies below 4.0 MeV. These, and other inelastic-scattering results, are described in detail in refs. 11 and 18, and are cited here only as ancillary experimental values.

The elastic-scattering results and their experimental uncertainties are summarized in Fig. 2. These results are in good agreement with the lower-energy (below 4.0 MeV) values previously reported from this laboratory (18). At higher energies there are few data for comparison. However, results have been reported at 8.05 MeV (19) and these are compared with the present 8.03 MeV values in Fig. 1. Overall, the two sets of data show qualitative consistency, but on close scrutiny sub-

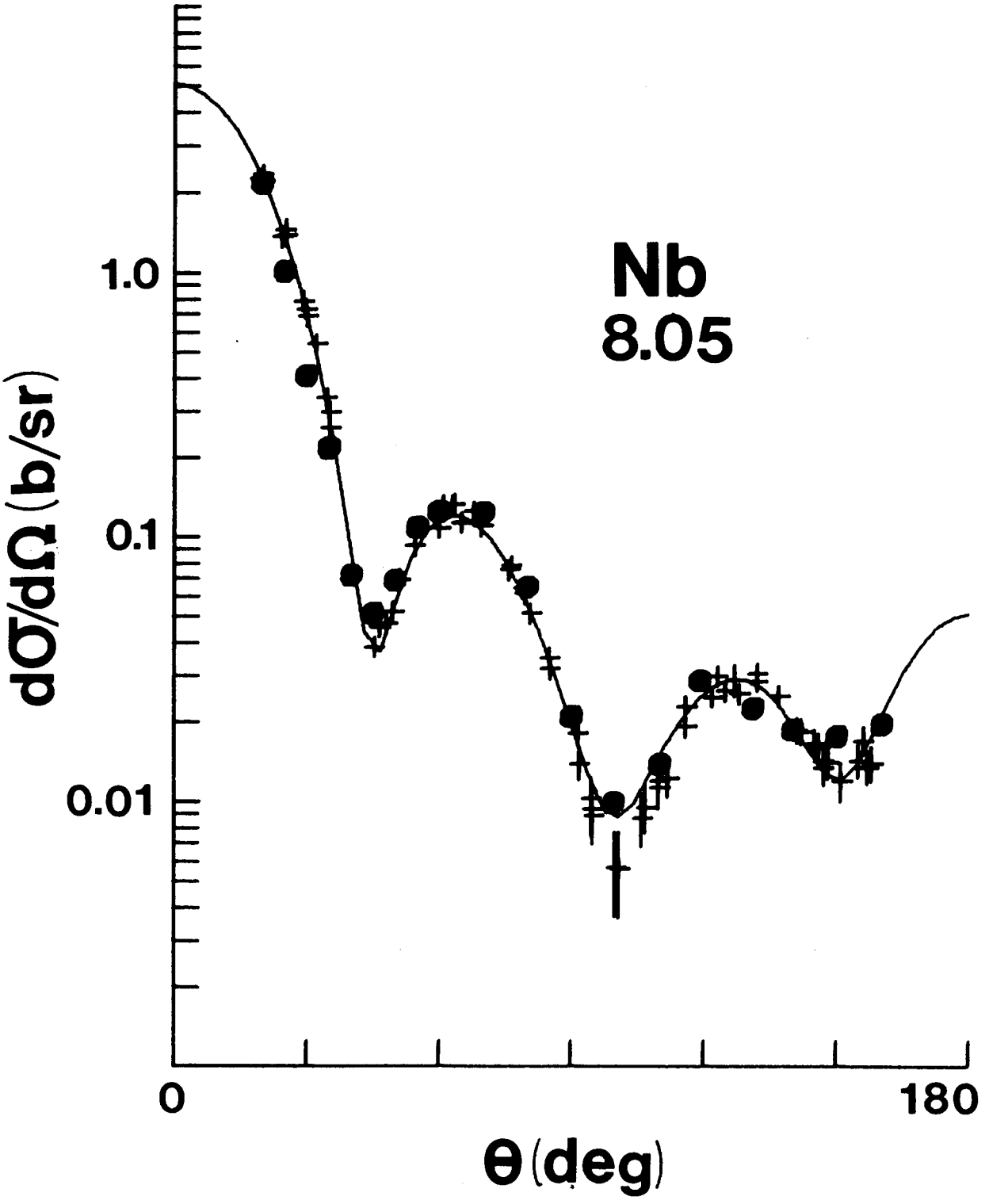

Fig. 1: Comparison of measured differential-elastic-scattering cross sections of niobium at a neutron energy of approximately 8.0 MeV. The present experimental results are indicated by "+" and those of ref. 19 by "●". The curve indicates the result of an optical-model calculation.

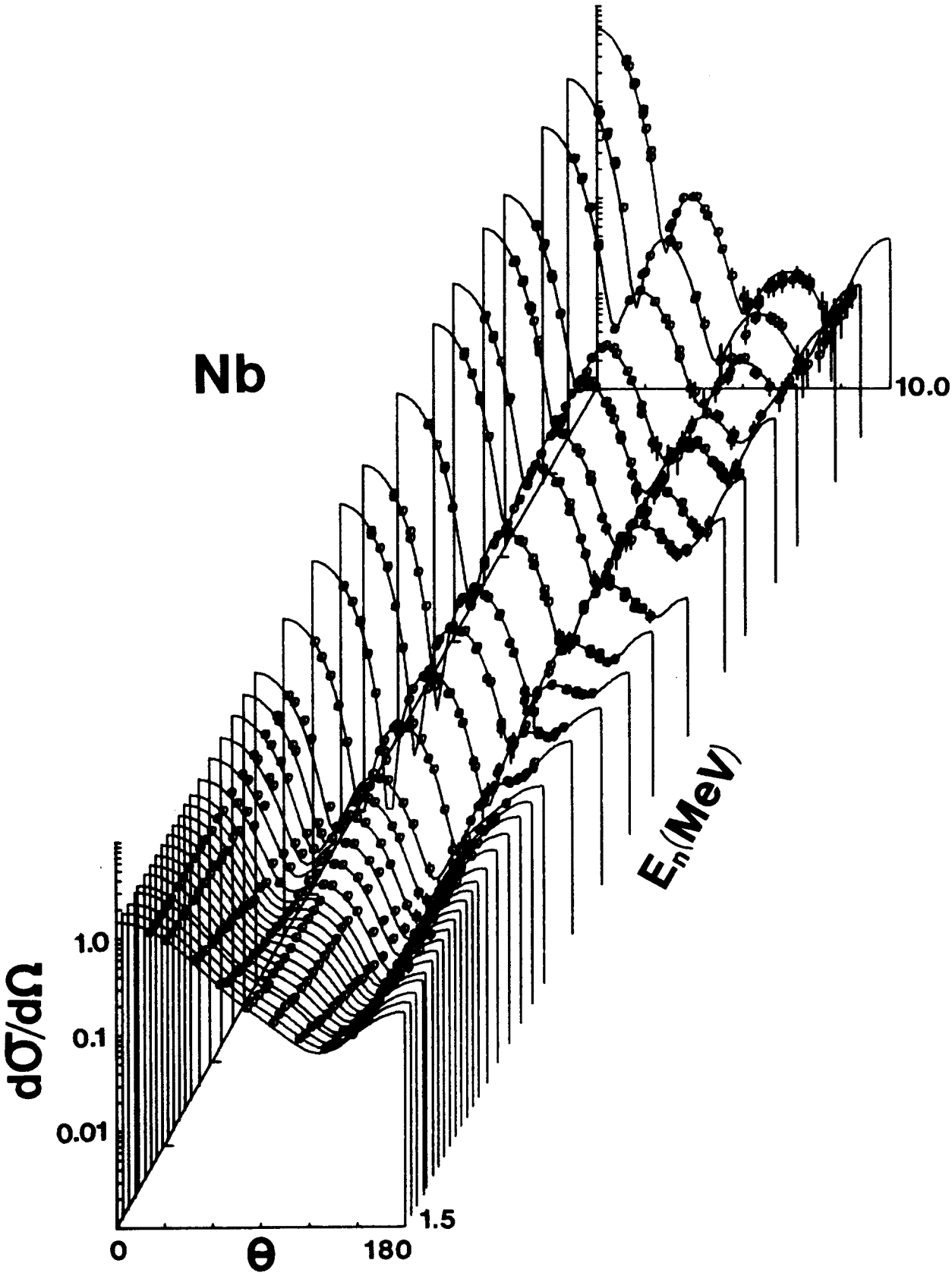

Fig. 2: Measured differential-elastic-scattering cross sections of niobium. The measured values are indicated by circular data symbols and the results of the optical-model calculations, discussed in the text, by curves. Cross sections are in b/sr and scattering angle (θ) in laboratory-system degrees.

stantive quantitative differences are revealed. Concurrent with all of the present measurements, the differential-elastic-scattering cross sections of carbon were measured. The resulting carbon angle-integrated elastic-scattering cross sections were consistent among themselves, and with the values given in ref. 20, to within several percent.

IV. INTERPRETATION

It was assumed that, in the energy region of interest, coupled-channels effects are unimportant and that the fast-neutron elastic-scattering and total cross sections of niobium could be described in terms of a spherical optical-statistical model (21). With that assumption, the energy dependence of the optical potential implied by the above experimental values was sought.

The OM parameters were determined by chi-square fitting the measured elastic-scattering distributions. The fitting procedure minimized

$$\chi^2 = \sum_i \left(\frac{\sigma_{expt}(\theta_i) - \sigma_{theo}(\theta_i)}{\delta\sigma_{expt}(\theta_i)} \right)^2, \qquad (1)$$

where the relevant experimental uncertainties were used. The latter are primarily of a statistical nature and thus are proportional to the square root of the cross section magnitudes. This is due to the particular experimental procedure employed, where entire angular distributions were obtained in a single measurement of a fixed duration. This is not a common method, and alternate fitting procedures are applicable to most other experimental results. It should be emphasized that the results of the fitting procedures are strongly dependent upon the applicable uncertainties, and the latter will depend upon the manner in which the experimental data are acquired. It was assumed that the real potential was of the Woods-Saxon form and the imaginary had the Woods-Saxon-derivative shape (22). A Thomas-type spin-orbit interaction was assumed, and its geometry was taken to be equal to that of the real potential. Although the strength of the spin-orbit interaction could have been varied, its exact value is ill defined by the present data. Consequently, the strength of the spin-orbit interaction was fixed at 6 MeV in the analysis. Selected fitting, varying the spin-orbit strength, supported this choice. The fitting was carried out using the computer code ABAREX (23), and

six para meters (real and imaginary potential depths, radii and diffusenesses) were varied. Below 6 MeV the compound-elastic contribution was significant. To calculate this the nine known discrete levels in ^{93}Nb below 1.1 MeV were taken into account. The spin and parity values were taken from ref. 24, with the 687- and 810-keV states assumed to be 3/2- and 5/2-, respectively. Above 1.1 MeV, the excitations were represented using the formalism and parameters of Gilbert and Cameron (25). The compound-elastic contribution was calculated using the Hauser-Feshbach formula (26), as modified by Moldauer (27). The observed "elastic"-scattering cross sections included a small inelastic component due to excitation of the 30-keV (1/2-) metastable level (17). ABAREX provides the option of fitting such composite "quasi-elastic"-scattering cross sections and that option was used. The contribution of the 30-keV level is very small throughout the range of the present experiments (9) and the results of the fitting were not sensitive to this inelastic component.

The low-energy (below 4.0 MeV) data may remain sensitive to residual fluctuations despite the relatively broad experimental resolutions and the averaging procedures outlined above. Thus, these low-energy distributions were concurrently fitted in two energy groups, extending from 1.5 to 2.9 MeV and from 3.0 to 4.0 MeV. The higher-energy distributions were individually fitted. Careful tests showed that compound-nucleus contributions had no effect on the results at energies above 6.0 MeV, and thus the fitting procedures assumed only shape scattering at these higher energies. The results of the initial six-parameter fits gave a relatively good determination of the real and the imaginary radii and thus they were fixed at 1.25 and 1.3 fm, respectively; approximately their average values as determined from the six-parameter fitting. The entire fitting procedure was then repeated keeping the radii fixed and varying the four remaining parameters. At the same time, the convergence criteria were somewhat tightened. The resulting average real and imaginary diffusenesses were 0.698 (±4.8%) and 0.465 (±9.0%) fm, where the uncertainties are defined as the root-mean-square deviation of the average values from their respective means. It should be noted that the potential strengths, expressed as the integral per nucleon (J), are sensitive to the the radii and, without confining them to reasonably stable values, six parameter fitting can lead to increased "spatter" of J values. Comparing J values deduced from potentials with considerably different radii is not particularly rewarding. The above fitting methodology was applicable to 9.0 MeV. From 9.0-10.0 MeV the elastic cross sections are very forward peaked and thus sensitive to the small uncertainties in the exact angular scale, cited above. These angular

uncertainties became the dominant factor in a region highly weighted in the fitting procedure, and they are not readily quantified. The problem was alleviated by including the measured neutron total cross sections, with a high weight, in the fitting of the 9.0, 9.5 and 10.0 MeV distributions. The total cross sections are very well known (9) and they provide a solid anchor for the fitting at forward angles. ABAREX has the capability for concurrently fitting neutron total and differential cross sections. For the higher-energy data, one can wonder whether or not there is evidence for a volume absorptive potential. This was investigated by including such a term in the fitting procedures. In all such cases, the fitting resulted in a volume strength consistent with zero.

In Fig. 3 are presented the volume integrals (28) of the real and imaginary potentials as obtained from this analysis, where

$$J_V = (4\pi/A) \int_0^\infty V(r) r^2 dr, \qquad (2)$$

with A the number of nucleons in the nucleus (in this case A=93). A similar expression holds for J_W, except that now the imaginary potential, W(r), is integrated. The volume integral J_W is less-well determined by the experimental data than is J_V. The estimated uncertainties in J_W are approximately 10% for the 9.0-10.0 MeV values and 7.5% at other energies. For J_V, the estimated uncertainty is somewhat less than 2% for all values. If one assumes that both J_V and J_W are constant as a function of energy, a least-square fit to the data gives J_V=(430.14±1.44) MeV-fm^3 with a normalized chi-square per point of 1.83, and J_W=(70.45±1.45) MeV-fm^3, with chi-square per point equal to 2.29. A significantly better fit is obtained if one introduces a linear energy dependence and writes

$$J_i = \alpha_i + \beta_i \cdot E, \qquad (3)$$

where E is the laboratory energy of the incident neutron in MeV. With this parameterization one obtains,

$$\alpha_V = (445.34 \pm 4.57) \text{ MeV-fm}^3$$
$$\beta_V = (-2.38 \pm 0.68) \text{ fm}^3 \qquad (4a)$$
$$\chi^2/\text{pt} = 0.96$$

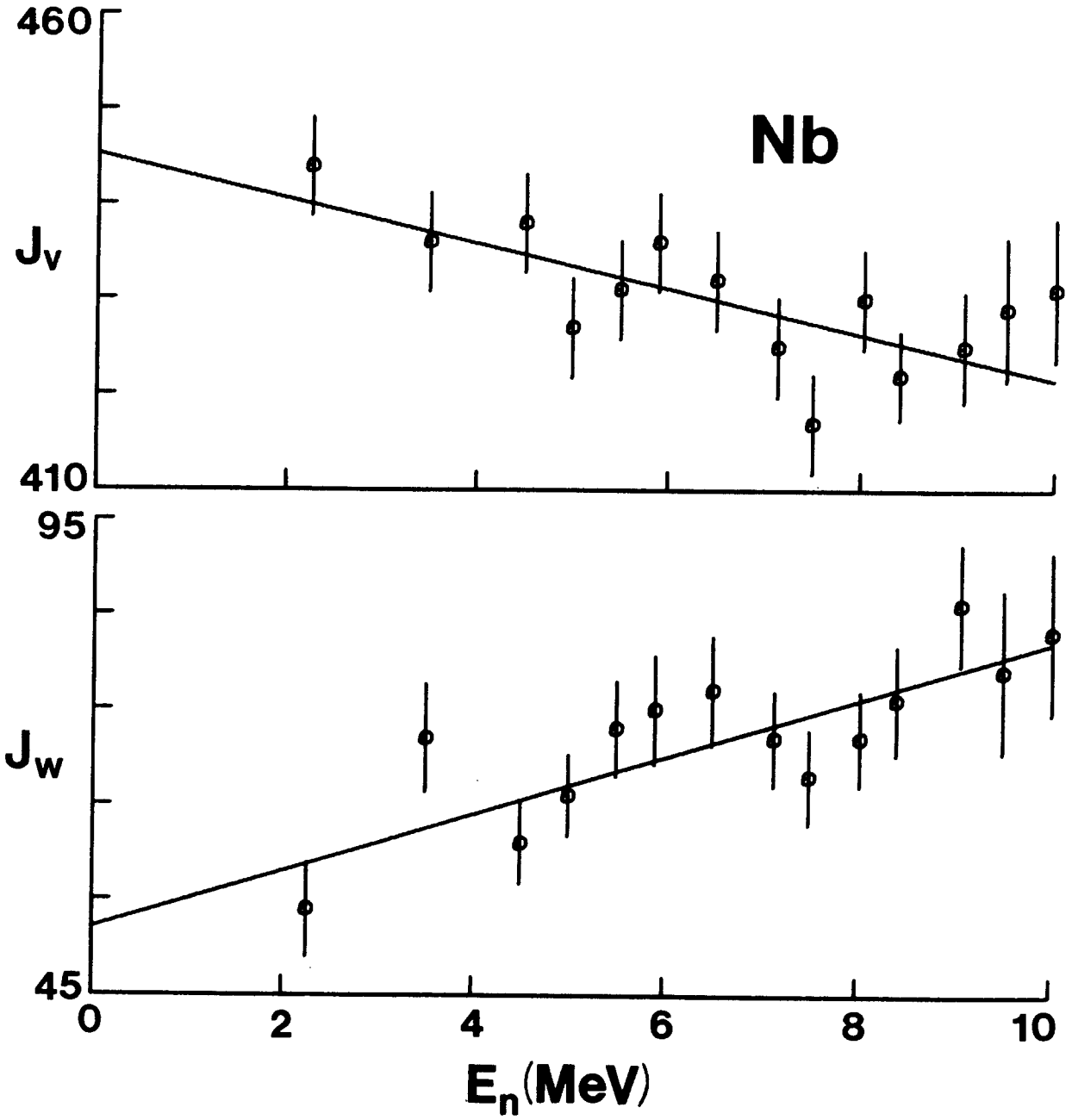

Fig. 3: Energy dependencies of the real, J_V, and imaginary, J_W, potential integrals per nucleon in units of MeV-fm^3. Circular symbols indicate the results deduced from the measurements and the curves the results obtained with the linear parameters of Eqs. 4a and 4b.

$$\alpha_W = (51.97 \pm 4.54) \text{ MeV-fm}^3$$

$$\beta_W = (2.99 \pm 0.70) \text{ fm}^3 \qquad (4b)$$

$$\chi^2/\text{pt} = 0.94,$$

and in both cases the uncertainties in α_i and β_i are almost exactly anti-correlated. The linear expressions of Eqs. 4 are descriptive of the values deduced from the measurements, as illustrated by the curves in Fig. 3.

The potentials obtained with the above fitting procedures gave a good description of the measured differential-elastic scattering, as illustrated by the curves of Fig. 2. Although the neutron total cross sections were used in the fitting procedure only at 9.0 MeV and above, the predicted total cross sections at energies less than 9.0 MeV are in excellent agreement with experiment (9), as can been seen from an inspection of Fig. 4. The result has the important consequence that Wick's limit (29) for the zero-degree scattering cross section was not violated in the analysis of the elastic-scattering data. In addition, the low-energy extrapolation of these potentials leads to a predicted s-wave strength function of 0.724 (in units of 10^{-4}) and a potential scattering length, R'=6.82 fm, in good agreement with the experimentally derived values, 0.60±0.07 and 6.9±0.1 fm, respectively (30). Thus it was concluded that the differential-elastic-scattering data, and other facets of the neutron interaction with niobium, from 1.5-10.0 MeV can be reasonably understood by using a real Woods-Saxon potential whose volume integral decreases slightly with energy and an imaginary surface-peaked derivative Woods-Saxon potential with a volume integral that increases with energy.

V. DISCUSSION

The value of β_V, given in the preceeding section, is somewhat smaller in magnitude than that found by Rapaport (1), who relied heavily upon proton-scattering data to obtain $\beta_V=(-2.9+0.2)$ fm^3 when $7 \leq E \leq 30$ MeV. The above α_V is within 2% of his ^{92}Mo value of 436 MeV-fm^3. There is only a weak dependence on the surface thickness, "a", for the volume integral of the real Woods-Saxon potential given by (1)

$$\frac{4\pi}{A}\int V(r)r^2dr \approx \frac{4\pi}{3} r_o^3 V_o \left[1 + \left(\frac{\pi a}{R}\right)^2\right], \qquad (5)$$

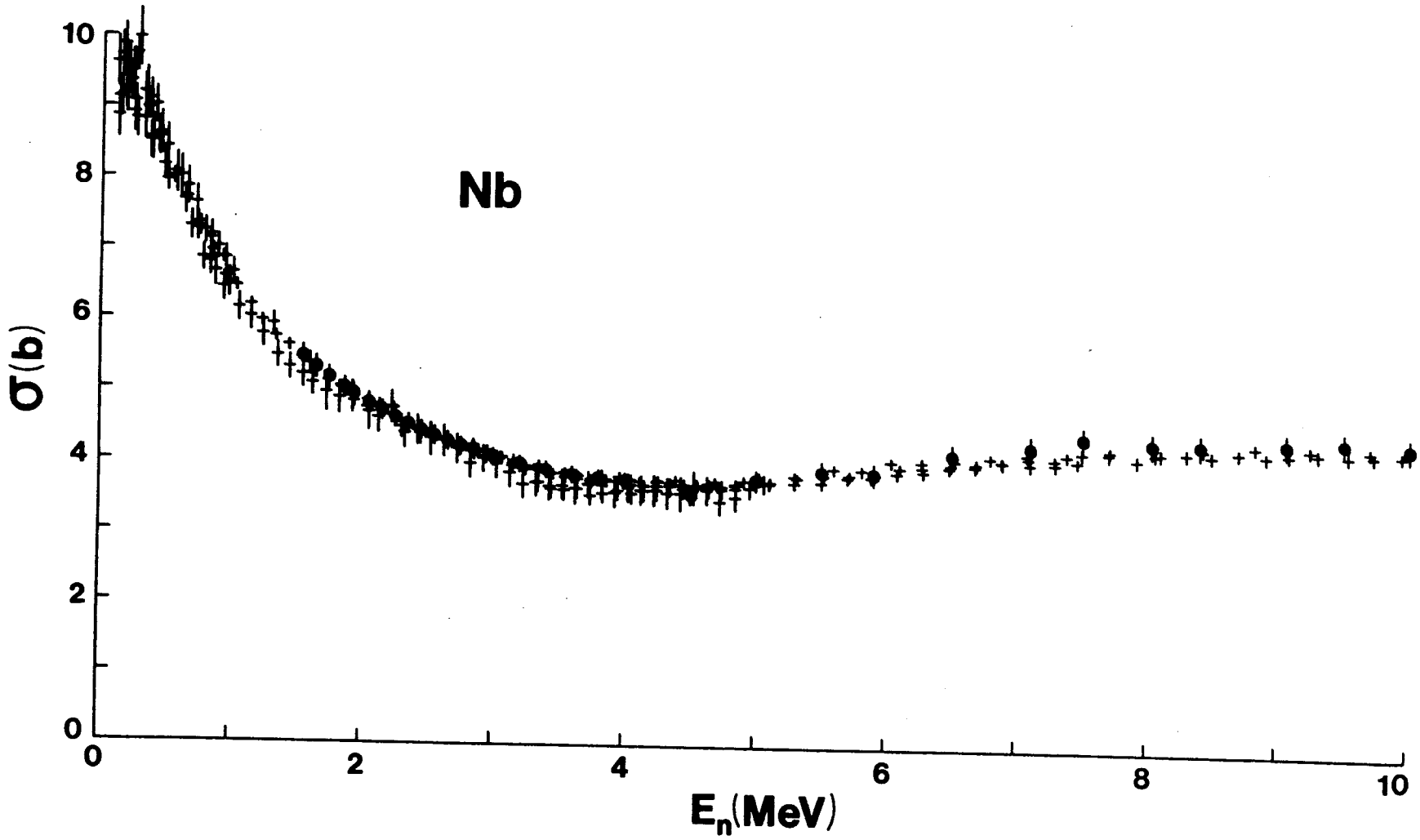

Fig. 4: Comparison of measured neutron total cross sections of niobium (+) (9) and those implied by the OM fits to the measured elastic scattering (●).

where $R=r_oA^{1/3}$ is the nuclear radius. Therefore, one can divide out the geometric factors that go into J_V using the average value, a=0.698 fm (obtained from the above scattering analysis), and obtain the well depth itself. With geometric factors of the present work

$$V_o = (47.34\pm0.49-(0.25\pm0.07)\cdot E) \text{ MeV} \quad . \tag{6}$$

On the other hand, the volume integral of the derivative Woods-Saxon well has a strong dependence on the diffuseness (1)

$$\frac{4\pi}{A}\int W(r)r^2dr \approx \frac{16\pi R^2 a}{A}\left[1+\frac{1}{3}\left(\frac{\pi a}{R}\right)^2\right]W. \tag{7}$$

Since the present values of the diffuseness vary by approximately ±9% about the rms value of a=0.465 fm, it is better to convert the Rapaport global imaginary potential to its integral values to make a comparison. With his parameters one finds for ^{93}Nb, that $(J_W)_{Rapaport}=(31.42+4.5\cdot E)$ MeV-fm^3. When $7 \leq E \leq 15$ MeV. Thus in the energy range where the two analyses overlap, the present imaginary potential is about 10% stronger than Rapaport's.

Turning now to the Fermi-surface anomaly, it was pointed out many years ago by Brown, Gunn and Gould (31) that near the Fermi surface the effective mass, m*, of a valence nucleon is nearly equal to its free mass, m. Evidence for this is provided by the fact that the energy spacing between valence shell model states is about that predicted by a static Woods-Saxon well (see for example, the calculations of Blomqvist and Wahlborn (32) on ^{208}Pb). The ratio (m*/m) can be shown to be related to the rate of change of the real potential with energy by (33)

$$(m^*/m)=1-(dV/dE). \tag{8}$$

Thus (m*/m) nearly equal to unity implies (dV/dE) is approximately zero near the Fermi surface. From consideration of the giant dipole resonance in Pb, Brown, Dehesa and Speth (2) speculated that an approximate expression for (m*/m) is

$$(m^*/m)=0.64+0.36\left(1+\left|E-E_f\right|/2\hbar\omega_o\right)^{-2} \quad , \tag{9}$$

where E_f is the Fermi energy and $\hbar\omega_o=41/A^{1/3}$ MeV. This ex-

pression has the property that $(m^*/m)=1$ at the Fermi surface (and consequently $dV/dE=0$) and goes over smoothly at high energies to the observed variation of J_V with E. This is illustrated by curve "B" in Fig. 5, where the normalization is adjusted to reproduce the neutron-scattering data indicated by the circular symbols.

On the other hand, Mahaux and Ngô (5) deduce the real part of the OM potential from the behavior of the imaginary part (34) via

$$V(r,E) = V(r) + \frac{P}{\pi}\int_{-\infty}^{\infty} \frac{W(r,E')}{E-E'}\,dE' \quad , \qquad (10)$$

where "P" implies the principal-value integral. For ^{40}Ca and ^{208}Pb they predict much more structure than the smooth variation of Eq. 9. For large positive values of E, the Mahaux-Ngô curve is similar to that given by Eq. 9. However, for E approaching zero their predicted curve goes above that of Eq. 9 and then drops below the prediction of Eq. 9 for E less than E_f, and finally rises again at still lower energies. From Fig. 5, one sees that the neutron-scattering data for niobium are consistent with the straight line fits of Eqs. 3 and 4a, or the curve of Eq. 9. At the lowest energies, at which a meaningful OM analysis can be made, there is no evidence for the marked nonlinearity predicted by Mahaux and Ngô for the doubly closed shell nuclei.

In order to investigate the above energy dependence further, one can consider the real potential necessary to give the correct binding energies of single particle states in this region. Nuclear structure studies near A=90 indicate that, to good approximation, ^{88}Sr can be considered a doubly-magic nucleus (35). Therefore, the available neutron stripping and pickup data on ^{88}Sr was used, together with tables of nuclear masses (36), to determine the experimental single-particle binding energies. For the $3s_{1/2}$ level in ^{89}Sr the data of Slater et al. (37) were used, whereas for all other states the results of Blok et al. (38) were used. The requisite binding energies in MeV are: -6.101 ($2d_{5/2}$), -4.77 ($3s_{1/2}$), -4.097 ($2d_{3/2}$) and -3.671 ($1g_{7/2}$) for the single-particle states relative to the ^{88}Sr core and -12.665 ($1f_{5/2}$), -12.238 ($2p_{3/2}$), -11.502 ($2p_{1/2}$) and -11.333 ($1g_{9/2}$) for the hole states. The depth of the Woods-Saxon potential necessary to reproduce these energies was then determined assuming a Thomas spin-orbit interaction with a strength of 6 MeV and a geometry identical to that of the Woods-Saxon well, (a=0.698 fm and r_o=1.25 fm, from the above neutron analysis). The isospin dependence of Rapaport's global model (1) implies that the ^{93}Nb potential should be 0.41 MeV deeper than that found for ^{88}Sr. When this is taken into account,

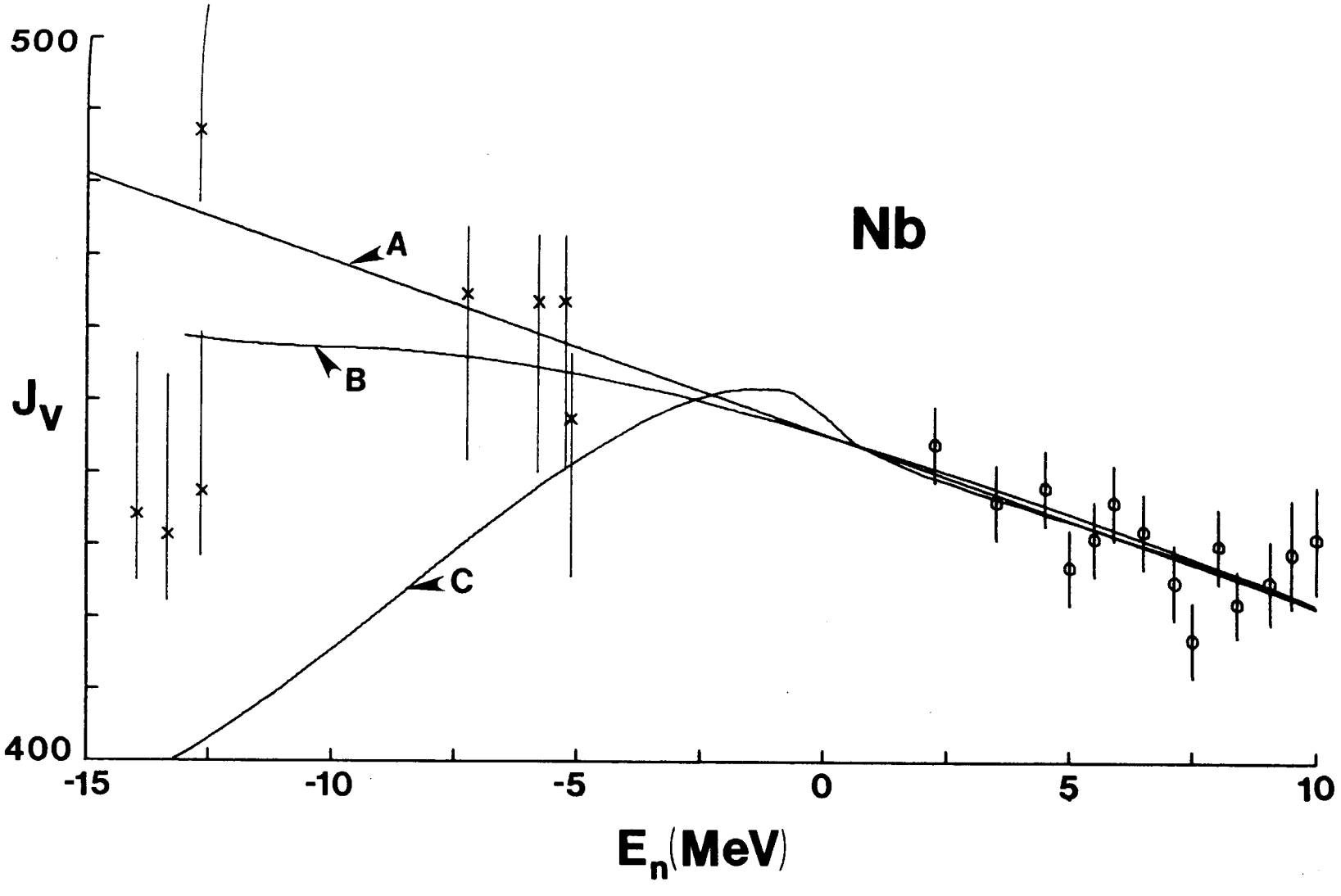

Fig. 5: The niobium real-potential integral per nucleon, J_V, at bound and unbound energies (in units of MeV fm^3). The positive-energy values are from the present experiment, those for the negative energies are deduced from particle and hole-state binding energies as discussed in the text. The curves denote: A=linear fit to the present neutron elastic-scattering results (Eqs. 3 and 4a), B=calculated from the theoretical expression of Brown et al. (2), Eq. (9), and C=calculated from Eq. 12 of the text.

together with the fact that the potential expands as $A^{1/3}$, the J_V results shown in Fig. 5 are obtained. The uncertainties that are assigned to the bound-state points reflect the fact that minor changes in the geometry of the well can change J_V by 2% without appreciably changing the binding energy. More important, any missed stripping strength would mean that the particle states are less tightly bound than we have assumed, leading to a smaller value of J_V, whereas any missed pickup strength would mean the hole states are more tightly bound leading to larger values of J_V. It is for these reasons than the uncertainties shown in Fig. 5 are asymmetric. It is conservatively estimated that the missed strength could change the binding energy by 1 MeV.

It is clear from Fig. 5 that, either extrapolating Eqs. 3 and 4a to negative energies or using the predictions based upon Eq. 9, one obtains equally acceptable fits to the volume integrals of the real potential needed to account for the binding energies of the $2d_{5/2}$, $3s_{1/2}$, $2d_{3/2}$ and $1g_{7/2}$ single-particle states. On the other hand, the hole states present conflicting evidence. The volume integral for the $1g_{9/2}$ hole state (J_V=487.13 MeV-fm^3) lies above the curve predicted by Eq. 9 but is consistent with a linear extrapolation of the fit to the scattering data. However, the remaining three hole states ($1f_{5/2}$, $2p_{3/2}$ and $2p_{1/2}$) fall below the curve predicted by Eq. 9 and about 10% below the straight-line fit to the scattering data. In fact, if it were not for the $1g_{9/2}$ integral, one might suspect that one is seeing the Mahaux-Ngô dip predicted to occur below the Fermi energy.

If W(r,E') does not vary wildly with E', one would expect from Eq. 10, that the variation of V with E should be strongly effected by the variation of W(r,E') with E' close to E (39). Therefore, an attempt was made to predict the behavior of the volume integral of the real potential, J_V, by making the following assumptions about J_W:

i) For $0 \leq E \leq 13.8$ MeV, assume J_W is given by the straight-line fit, Eqs. 3 and 4b.

ii) For $13.8 \leq E \leq 30$ MeV, W is assumed to be given by Rapaport's global imaginary interaction (1), which contains both surface and volume absorption. In terms of the volume integral of W, this becomes

$$J_W = 101.87 - 0.622 \cdot E \text{ MeV-fm}^3. \qquad (11a)$$

The reason for the choice of 13.8 MeV for connecting i) and ii) is that at this energy J_W given by the two separate expressions has the same value.

iii) On the basis of the dilute Fermi gas model, it can be shown (5,40) that, for E close to the Fermi energy E_f, W is proportional to $(E-E_f)^2$. For ^{93}Nb, E_f is approximately -10 MeV and it is assumed that

$$J_W = 0.51965\ (E+10)^2\ \text{MeV-fm}^3, \tag{11b}$$

for $-20 \leq E \leq 0$.

With these assumptions, J_W has a continuous value in the energy range $-20 \leq E \leq 30$ MeV, and when these expressions are inserted in Eq. 10 one predicts that

$$J_V(E) = J_o + \frac{1}{\pi}\left\{ 0.51965\left[20E + (E+10)^2 \ell n \left|\frac{E}{20+E}\right|\right] + (51.965+2.9946E)\ell n \left|\frac{13.8-E}{E}\right| + (101.87-0.622E)\ell n \left|\frac{30-E}{13.8-E}\right|\right\}, \tag{12}$$

where J_o is a constant. For a best fit to the scattering data, J_o=432.81 MeV-fm^3 and the resulting chi-square per point is 0.997.

In Fig. 5, curve "C" represents Eq. 12. It is clear that an optical-model fit to the neutron-scattering data of niobium in the energy range 2 to 10 MeV does not distinguish between the three fits to the J_V data: A) the linear fit which gives a normalized chi-square per point of 0.959, B) the curve generated from Eq. 9 which gives a chi-square of 0.925, and C) the "first principles curve" of Eq. 12. In contrast to ^{40}Ca and ^{208}Pb, where deviations of J_V from linearity are predicted to occur in the neighborhood of E=10 MeV, such departures are predicted at energies below 500 keV for ^{93}Nb. Even when $E \to 0$, it is difficult to distinguish experimentally between the three curves shown in Fig. 5. For example, when the dispersion relation value for J_V is used, the s-wave strength function and scattering length are predicted to be 0.688 and 6.69 fm, respectively, and this is only a minor change from the values given when Eqs. (3) and (4a) are used, 0.724 and 6.82 fm.

The bound-state data (particularly the hole-state values of J_V) present a conflicting picture. If one were to leave out the $1g_{9/2}$ point (and there is no apriori reason for doing so), one can see that a curve similar to that given by Eq. 12 might reasonably well go through the experimental points. However, in order to fit the data a more sophisticated parameterization than that of Eq. 11b will have to be made for W when $E \leq 0$. The predicted behavior of J_V for E=2.25 to 10 MeV is, of course, affected by the choice of Eq. 11b. However, even when W is set equal to zero for $E < 0$ (corresponding to a discontinuity in J_W and giving rise to a logarithmic singularity in J_V as E 0) the normalized chi-square per point for the scattering data only changes to 1.346.

VI. CONCLUDING COMMENTS

Detailed measurements of the neutron differential-elastic-scattering cross sections of niobium have been made from 1.5 to 10.0 MeV, and these provide a sound basis for the deduction of spherical optical-model parameters. These parameters provide a good energy-dependent description of the observed elastic scattering and the independently measured neutron total cross sections, and give a very reasonable value for the s-wave strength function and potential scattering length. The volume integral per nucleon of the real potential, J_V, decreases with increasing energy in a manner that is consistent with a linear behavior, whereas the analogous quantity for the imaginary potential increases linearly with energy. The consistency of the analysis of the data is demonstrated by using the observed E dependence of the imaginary potential integral, J_W, to predict the observed E dependence of J_V. In contrast to ^{40}Ca and ^{208}Pb, where a marked deviation from a linear E dependence at unbound energies is predicted for J_V (5), none is observed or predicted in niobium.

ACKNOWLEDGEMENTS

The authors are indebted to a number of members of the Applied Physics Division, Argonne National Laboratory, for their assistance in various aspects of this work.

References

1. J. Rapaport, Phys. Reports, 87 25 (1982).

2. G. Brown, J. Dehesa and J. Speth, Nucl. Phys. A330 290 (1979).

3. M. Bauer, E. Hernandez-Saldana, P. E. Hodgson and J. Quintanilla, J. Phys. G8 525 (1982).

4. P. E. Hodgson, Proc. International Sym. on Nucl. Phys. at Large Tandem Accelerators, Legarno (1983); also Oxford Report 22/83 (1983).

5. C. Mahaux and H. Ngô, Nucl. Phys. A378 205 (1982); Phys. Letters, 100B 285 (1981).

6. R. W. Finlay, J. R. M. Annand, J. S. Petler and F. S. Dietrich, AIP Conference Proceedings No. 124 edited by J. Rapaport, R. W. Finlay, S. M. Grimes and F. S. Dietrich, American Institute of Physics, 1985 p. 322; Phys. Letters, to be published.

7. See for example, J. Reber and J. Brandenberger, Phys. Rev. 163 1077 (1968).

8. See for example, G. Haouat, J. Lachkar, Ch. Lagrange, Y. Patin, J. Sigaud and R. Shamu, CEA Report, NEANDC(E)-196 "L" (1978).

9. A. Smith, D. Smith and R. Howerton, Argonne National Laboratory Report, ANL/NDM-88 (1985).

10. J. Meadows and D. Smith, Argonne National Laboratory Report, ANL-7938 (1972).

11. A. Smith, P. Guenther and J. Whalen, Argonne National Laboratory Report, ANL/NDM-70 (1982).

12. A. Smith, P. Guenther, R. Larson, C. Nelson, P. Walker and J. Whalen, Nucl. Instruments and Methods 50 277 (1967).

13. A. Smith, P. Guenther and R. Sjoblom, Nucl. Instruments and Methods 140 397 (1977).

14. A. Smith and P. Guenther, Argonne National Laboratory Report, ANL/NDM-63 (1982).

15. Nuclear Standards File, IAEA Tech. Report 227, Editors A. Smith, H. Conde and A. Lorenz, IAEA Press, Vienna (1983).

16. P. Guenther, Ph.D. Thesis, Univ. of Illinois (1977).

17. Table of Isotopes, 7th edition, C. Lederer and V. Shirley, John Wiley and Sons, New York (1978).

18. A. Smith, P. Guenther and J. Whalen, Z. Phys. 264 279 (1973).

19. B. Holmqvist and T. Wiedling, Aktiebolaget Atomenergi Report, AE-430 (1971).

20. C. Fu and F. Perey, At. Data and Nucl. Data Tables 22 249 (1978).

21. P. E. Hodgson, Nuclear Reactions and Nuclear Structure, Clarendon Press, Oxford (1971).

22. See for example, F. G. Perey, Nuclear Spectroscopy and Reactions, edited by J. Cerny, Academic Press, N.Y. (1974) part B, p. 137.

23. ABAREX, A Spherical Optical Model Code, P. A. Moldauer, Priv. Com. (1983).

24. I. J. Van Heerden, W. R. McMurray and R. Saayman, Z Physik, A260 9 (1973).

25. A. Gilbert and A. Cameron, Can. Jour. Phys. 43 1446 (1965).

26. W. Hauser and H. Feshbach, Phys. Rev. 87 366 (1952).

27. P. A. Moldauer, Nucl. Phys. A344 185 (1980).

28. H. Feshbach, Ann. Rev. Nucl. Sci. 8 49 (1959).

29. See for example, page 91 of ref. 21.

30. S. Mughabghab, M. Divadeenam and N. E. Holden, Neutron Cross Sections, Vol.-1, Part-A, Academic Press, N.Y. (1981).

31. G. E. Brown, J. H. Gunn and P. Gould, Nucl. Phys. 46 598 (1963).

32. J. Blomqvist and S. Wahlborn, Ark. Fys. 16 545 (1960).

33. See for example G. R. Satchler, Direct Nuclear Reactions, Clarendon Press, Oxford, 1983, Appendix B p. 820.

34. G. R. Satchler, op.cit. p. 58.

35. F. J. D. Serduke, R. D. Lawson and D. H. Gloeckner, Nucl. Phys. A256 45 (1976).

36. A. H. Wapstra and K. Bos, Atomic Data and Nuclear Data Tables 19 177 (1977).

37. D. C. Slater, E. R. Cosman and D. J. Pullen, Nucl. Phys. A206 433 (1973).

38. H. Blok, W. R. Zimmerman, J. J. Kraushaar and P. A. Batay-Csorba, Nucl. Phys. A287 156 (1977).

39. M. A. Nagarajan, C. C. Mahaux and G. R. Satchler, Phys. Rev. Lett. 54 1136 (1985).

40. R. Sartor and C. Mahaux, Phys. Rev. C21 1546 (1980).